Research Square

Preprints are preliminary reports that have not undergone peer review.
They should not be considered conclusive, used to inform clinical practice,
or referenced by the media as validated information.

Influence of Electrolyte Concentration on the Morphology and Airborne Particulate Matter Removal Efficiency of Electrodeposited Copper Films

R. S. Sidharaddi

raju24physics@gmail.com

Dr. A. P. J. Abdul Kalam Research Laboratory, Yashavantrao Chavan Institute of Science

A. A. Mane

Sant Gajanan Maharaj College of Engineering

P. S. Maldar

Rajarambapu Institute of Technology, Affiliated to Shivaji University Kolhapur

S. P. Desai

KITS College of Engineering (Autonomous)

M. H. Nadaf

Sant Gajanan Maharaj College of Engineering

A. B. Farakte

Sant Gajanan Maharaj College of Engineering

A. S. Selmokar

Sant Gajanan Maharaj Rural Polytechnic

S. A. Nikam

Sant Gajanan Maharaj College of Optometry

V. S. Sawant

Dr. A. P. J. Abdul Kalam Research Laboratory, Yashavantrao Chavan Institute of Science

Research Article

Keywords: Cu Films, Electrodeposition, Nodular microstructure, Electrostatic Air Purifier (EAP)

Posted Date: August 6th, 2026

DOI: https://doi.org/10.21203/rs.3.rs-10126181/v1

License: This work is licensed under a Creative Commons Attribution 4.0 International License.
Read Full License

Additional Declarations: No competing interests reported.

Influence of Electrolyte Concentration on the Morphology and Airborne Particulate Matter Removal Efficiency of Electrodeposited Copper Films

R. S. Sidharaddi [a, b, *], A. A. Mane [c], P. S. Maldar [d], S. P. Desai [e], M. H. Nadaf [c], A. B. Farakte [c], A. S. Selmokar [f], S. A. Nikam [g], V. S. Sawant [a, h]

[a] Dr. A. P. J. Abdul Kalam Research Laboratory, Department of Physics, Yashavantrao Chavan Institute of Science, Satara, M.S., 415 001, India

[b] Government Polytechnic, Miraj, M.S., 416 410, India

[c] Sant Gajanan Maharaj College of Engineering, Mahagaon, M.S., 416 503, India

[d] Rajarambapu Institute of Technology, Affiliated to Shivaji University Kolhapur, Rajaramnagar, Islampur, M.S., 415414, India

[e] KITS College of Engineering (Autonomous), Gokul Shirgaon, Kolhapur 416 234, M.S., India

[f] Sant Gajanan Maharaj Rural Polytechnic, Mahagaon, M.S., 416 503, India

[g] Sant Gajanan Maharaj College of Optometry, Mahagaon, M.S., 416 503, India

[h] Air Ion Laboratories, D. P. Bhosale College, Koregaon, M.S., 415 001, India

*** Corresponding author:** raju24physics@gmail.com;

Abstract

Copper nodules were deposited onto steel substrates using the electrodeposition technique. XRD analysis confirmed that the films are polycrystalline with a face centered cubic crystal structure. SEM revealed the formation of a nodular microstructure. AFM results showed that both the mean particle size and root mean square surface roughness increased with solution concentration from 86.52 nm to 224.55 nm and 23.44 nm to 76.19 nm, respectively before decreasing to 168.5 nm and 45 nm at higher concentrations. The film produced at a bath concentration of 0.075 M exhibited a thickness of 721 nm, along with the highest performance: a particulate removal efficiency of 88.78% for dhoop smoke and an air purifying factor (AFC) of 54.12 over 405 s of operation. This performance surpassed that of stainless steel discharging rod. Finally, the study provides a detailed analysis of particulate matter (PM) removal within an enclosed room using the developed air purifier.

Keywords: Cu Films; Electrodeposition; Nodular microstructure; Electrostatic Air Purifier (EAP)

1. Introduction

Incense burning practices, such as dhoop, agarbatti, and diya, are widely prevalent across Asian countries, particularly in India, especially in places of worship. However, incomplete combustion of incense releases a variety of pollutants, including hazardous volatile organic compounds (VOCs), nitrogen oxides (NO_x), and fine to ultrafine PM **[1]**. Exposure to these contaminants through inhalation can lead to serious health effects, including diabetes, cognitive impairment such as memory loss, symptoms of depression, and cardiovascular and respiratory diseases. Incense burning in places of worship significantly increases PM concentrations, often exceeding the limits set by the World Health Organization and other regulatory bodies. Therefore, controlling indoor air conditions is essential to reduce public exposure to harmful PM **[2]**. The primary approach to reducing fine PM involves improving air circulation and using air cleaning or purification systems. These particles can be effectively removed from indoor environments using various air purification technologies, including EAPs, high efficiency particulate air (HEPA) filters, fabric filters, mechanical collectors, and electrostatic precipitators (ESPs) **[3].**

Copper (Cu) thin films have a wide range of applications owing to their superior electrical conductivity compared to aluminum (Al) and their attractive appearance **[4]**. Due to their excellent adhesion to rubber, electroplated Cu and its alloys are widely used in decorative applications as well as in the tyre industry **[5]**. Various techniques are employed to deposit Cu thin film coatings, including the Ultra violet (UV) photodeposition **[6]** electrodeposition **[7]**, chemical co-deposition **[8]**, and Chemical vapor deposition **[9].** The electrodeposition method was chosen among these techniques due to its simplicity, cost effectiveness, ability to coat at room temperature, capability to achieve controllable and uniform layer thickness, high deposition efficiency, and relatively low toxicity **[10, 11].** The deposition parameters of thin films play a critical role in determining their physicochemical properties, including crystal structure, surface morphology, and thermal stability. The careful control of these deposition variables governs the performance and functionality of electroplated metals and alloys **[12]**. Several factors including bath composition and type, solvent concentration, electrode design, pH, applied potential, deposition temperature, deposition time, current density, and the use of additives can influence the nucleation and growth processes, as well

as the uniformity of thin film surfaces **[13-15].** Wu et al. **[16]** were produced twinned Cu thin films by DC electrodeposition using mercapto propanesulfonate (MPS), gelatin, and SPS additives, where MPS enhanced twin formation through increased Cu^{+} intermediates. The resulting high twin boundary density improved (111) texture, reduced stress, and enhanced mechanical performance, achieving 96% (111) orientation and a hardness of 1.91 ± 0.04 GPa at 50 ASD. Kim et al. **[17]** investigated the effect of Cu bath concentration on thin film fabrication and found that the solution concentration significantly influences the film's porosity and contamination levels. Yildirim et al. **[18]** studied the impact of Cu concentration on the optical and dielectric properties of $Cu_xZn_{1-x}S$ thin films. Therefore, it is essential to investigate how electrodeposition parameters influence the chemical and physical properties of Cu thin films.

In this study, Cu thin films were successfully electrodeposited onto stainless steel (SS) substrates using solution concentrations ranging from 0.025 M to 0.100 M to enhance ion emission, particulate removal efficiency (PRE), and the air cleaning factor (ACF) for dhoop PM. The physical and chemical properties of the electroplated Cu films were analyzed as a function of solution concentration. Furthermore, the influence of these physicochemical characteristics on the air cleaning performance of the electrostatic air purifier (EAP) was investigated.

2. Experimental

2.1 Synthesis and characterization of Cu thin films

Substrate cleaning is a critical step in depositing thin films with consistent properties, as it removes chemical bonds that attach contaminants to the substrate surface. To ensure reproducible film characteristics such as uniformity, adhesion, and controlled porosity, the substrate must be thoroughly cleaned to eliminate impurities without causing any damage. The substrate cleaning method depends on the substrate material, the required level of purity, and the nature of the impurities to be removed. Proper cleaning of the substrate surface significantly influences both the adhesion and the quality of the resulting thin film. Several cleaning methods can be applied to SS surfaces, depending on the type of contaminants and the substrate structure. In this study, SS plates with dimensions of 7 × 1 × 0.2 cm^3 were used as substrates for thin film deposition. Prior to deposition, the substrates were carefully polished. They were then cleaned with mild detergent solutions followed by rinsing with double distilled water (DDW). To remove remaining dirt and dust particles, the substrates were treated in a 0.25 M NaOH solution containing a surfactant at

70 °C for 15 minutes. Finally, the substrates were annealed in methanol vapors to complete the surface preparation.

Cu thin films were electroplated using a conventional three electrode setup with a non agitated deposition bath. The SS substrates served as the working electrode, graphite was used as the counter electrode, and a saturated calomel electrode functioned as the reference electrode. **Fig. 1** shows schematic of electrodeposition method. Analytical reagent grade copper sulphate ($CuSO_4 \cdot 5H_2O$), a moisture-sensitive blue crystalline powder, was obtained from Sisco Research Laboratories Pvt. Ltd., Taloja, Maharashtra. Additionally, white crystalline sodium citrate tribasic dihydrate ($C_6H_5Na_3O_7 \cdot 2H_2O$) was also procured for use in the study. Solutions of copper sulphate ($CuSO_4$) with concentrations of 0.025 M, 0.050 M, 0.075 M, and 0.100 M were prepared by dissolving 1.25 g, 2.5 g, 3.75 g, and 5.0 g of $CuSO_4$, respectively, in 200 mL of DDW. Additionally, a 50 mL sodium citrate solution with a concentration of 0.200 M was prepared by dissolving 2.93 g of powdered $C_6H_5Na_3O_7 \cdot H_2O$ in DDW. Sodium hydroxide (NaOH) was used to adjust the pH of each $CuSO_4$ coating bath to approximately 6.5. Cu electroplating was then carried out using $CuSO_4$ solutions of varying concentrations for an optimized deposition time of 30 min. For convenience, the samples were coded as CC_1, CC_2, CC_3, and CC_4, corresponding to $CuSO_4$ concentrations of 0.025 M, 0.050 M, 0.075 M, and 0.100 M, respectively. All other electrodeposition parameters were kept constant throughout the coating process. After deposition, the films were allowed to dry naturally, then stored in butter paper prior for characterization.

XRD analysis was performed to determine the crystal structure of the Cu films. The surface morphology was examined using SEM, while the surface topography and roughness of the coatings were analyzed through AFM. **Fig. 2** represents the experimental setup of dhoop smoke with EAC. The Cu thin film, functioning as the discharging rod in the EAP, was evaluated using a custom built high voltage DC source of ±8500 V and an air ion counter. The concentration of air ions generated by the corona discharge was measured with the ion counter. The AQI Monitor measures the real time air quality. In addition to the formaldehyde detection, the temptop detector is utilized to identify particle concentrations between 2.5 and 10 μm. A Teflon spacer, nut, and Cu thin film electrode were installed into a Nylon rod. To protect the circuit from sparking under varying environmental conditions, a white enclosure and high voltage insulating resin were used. Experiments were conducted in two sealed glass chambers of identical dimensions. Dhoop smoke was generated inside the testing chamber from its source for air purification evaluation. A 2 mW

helium neon laser beam with a wavelength of 6300 Å was used as the light source for the experiments. Initially, a standard glass chamber containing dhoop smoke was employed to perform a reference test for visibility. The laser beam was directed through the standard chamber containing dhoop smoke. Sensors and other electrical instruments were positioned on the opposite side of the chamber. A light meter was used to evaluate visibility by measuring the transmitted light intensity.

3. Results and discussion

3.1 X Ray Diffraction

Fig. 3 shows the XRD patterns of Cu films deposited at different bath concentrations. Comparison with the standard JCPDS card No. 00-004-0836 and the measured interplanar spacing (d) confirms that the electroplated Cu films are polycrystalline with a face centered cubic (FCC) crystal structure. The sharp, well defined peaks corresponding to the (111), (200), and (220) planes indicate the high crystallinity of the Cu films. The pronounced intensity of the (111) reflection suggests a preferred orientation of the layered structure along the [111] direction. It is observed that the intensity of the (111) plane increased with bath concentration from 0.025 M to 0.075 M, but decreased at 0.100 M. The CC_3 sample exhibited the highest (111) peak intensity among all specimens, with a 2θ value of 43.4°, indicating a significant enhancement in the crystallinity of the film. The CC_4 sample exhibited a high deposition rate, which resulted in the formation of a loosely adhering powdery thin layer, causing a reduction in the peak intensities of the (111), (200), and (220) planes. The relatively low intensity diffraction peaks of the (200) and (220) planes at 2θ = 50.4° and 74.1°, respectively, indicate that crystal growth along these directions occurs more gradually. Similar results have been reported by other researchers **[19-20].** The crystallite size (D) of the copper films is calculated using Debye-Scherer's equation as **[21]**

$$D = \frac{0.9\lambda}{\beta . \cos\theta} \dots\dots\dots\dots\dots\dots\dots\dots\dots\dots\dots\dots\dots\dots\dots\dots (1)$$

where λ is X-ray wavelength, β is full width at half maximum (FWHM), and θ is Bragg angle. **Table 1** presents the crystallite sizes of the Cu films. The crystallite size of the (111) plane increased from 52.3 nm to 62.7 nm as the bath concentration was raised from 0.025 M to 0.075 M. This growth is attributed to the coalescence and merging of smaller crystallites, which enhances the crystallinity of the films. In contrast, the CC_4 sample exhibited a reduced (111) crystallite size

of 34.6 nm, likely due to the formation of a loosely adhering, powdery coating resulting from the high deposition rate on the substrate surface.

3.2 Morphological Analysis

The SEM images of Cu films deposited at different solution concentrations are shown in **Fig. 4**. The electroplated Cu films exhibit nodular, well organized surface morphologies. It is observed that as the solution concentration increased from 0.025 M to 0.075 M, the film growth rate increased, promoting the formation and assembly of nodular structures. In the CC_1 sample, the nodules are uniformly distributed and closely packed. For the CC_2 sample, the increased material deposition over the same area results in a denser surface structure, with more compact nodules and smaller pores. At the optimal bath concentration for the CC_3 sample, the nodules grow significantly, with diameters ranging from 53 to 70 nm. The irregular distribution of nodules across the film surface creates microscopic pores of varying sizes, which enhance ion discharge and, consequently, improve the air purification performance. In contrast, the CC_4 sample shows a dense aggregation of circular grains rather than the typical nodular surface morphology. **Fig. 5** shows SEM images of CC_3 Cu thin film at different magnifications: i) x 2000, (ii) x 5000, (iii) x 10000, and (iv) x 20000. It clearly revealing the hierarchical nodular architecture and pore distribution at higher magnifications.

3.3 Topographical Analysis

The AFM micrographs of Cu films deposited at different bath concentrations are shown in **Fig. 6,** and **Table 2** summarizes the corresponding average particle size and RMS surface roughness. As the bath concentration increased from 0.025 M to 0.075 M, the mean particle size of the copper films increased from 86.52 nm to 224.55 nm, while the RMS surface roughness rose from 23.44 nm to 76.19 nm. At a bath concentration of 0.100 M, both the RMS roughness and mean particle size decreased to 45 nm and 168.5 nm, respectively. During electroplating, small particles agglomerate and coalesce into larger ones, leading to an increase in particle size and an enhancement of the surface roughness of the films. The random distribution of nodules in the CC_3 sample further increases the surface area, as confirmed by SEM micrographs. Consequently, the enhanced surface morphology of the CC_3 sample facilitates significant ion discharge, improving the purification of air containing dhoop PM. In contrast, the CC_4 sample shows a reduction in surface roughness due to the formation of uneven, powdery coatings.

3.4 Electrostatic Air Purifying Characteristics for Cu films

3.4.1 Determination of concentration of smoke particulate matter and PRE

The light intensity was measured every 15 sec. Visibility increased noticeably over time due to the negative ions generated by the EAP within the chamber. At 15 sec intervals, the concentration of dhoop particles was calculated using the Beer–Lambert law as follows **[22]**:

$$I = I_0 e^{-\alpha m} \ldots\ldots\ldots\ldots\ldots\ldots\ldots\ldots\ldots\ldots\ldots\ldots (2)$$

Where, I and I_0 are observed and incident intensity of light respectively, m number of particles and α scattering cross-section of fog or smoke. **Table 2** shows that the transmitted light intensity increases with bath concentration from 0.025 M to 0.075 M, but decreases at 0.100 M. The CC_3 film reaches 50% of the transmitted light in 75 sec, demonstrating a faster response than both the SS substrate and the other Cu films. The concentration of dhoop PM decreases exponentially over time when the EAP is operated. The particle removal efficiency (PRE) is highest for the CC_3 film, which was prepared at a 0.075 M bath concentration. **Fig. 7** illustrates Concentration of particles versus time for dhoop PM using EAP. It shows natural disintegration of smoke PM within the glass chamber over time. The CC_3 film shows enhanced PM removal due to its increased surface area and surface roughness, which promote a higher rate of ion generation. This enhancement in air purification has also been confirmed through SEM, XRD, and AFM analyses. Sawant et al. **[23]** reported similar trends for fog PM. The rapid response time of the EAP using the CC_3 discharging rod may be attributed to the efficiency of the EAP, the chamber volume, or the type of discharging rod employed.

The dhoop smoke disintegration concentration is determined when (1) EAP is turned off [$C_{Natural}$ (Pm, t)] (2) EAP is turned on [C_{EAP} (Pm, t)] using the formula **[23, 24]**

$$\text{Particle Removal Efficiency (PRE)}\% = \frac{\text{CNatural (Pm, t = 0)} - \text{CEAP (Pm, t)}}{\text{CNatural (Pm, t = 0)}} \text{X } 100 \ldots (3)$$

Fig. 8 shows efficiency for removing particles verses time of dhoop PM for various concentrations of solvents. It indicates the PRE over time for dhoop PM using Cu films and a SS rod in the EAP. The PRE increases due to the ionic environment generated by the EAP. Cu coated EAP rods exhibit higher PRE values for dhoop particles compared to SS rods. **Table 2** shows that the PRE increases from 74.87% to 88.78% as the solution concentration rises from 0.025 M to 0.075 M. For the CC_4 film, PRE decreases to 81.09% due to the formation of a powdery coating, which likely reduces

ion generation and, consequently, the efficiency of particle removal. The highest PRE observed for the CC_3 film is attributed to its enhanced surface structure, which facilitates a higher rate of ion generation, as confirmed by AFM analysis. Similar findings were previously reported by Pushpawela et al. **[25]**. Therefore, the bath concentration during electrodeposition of the Cu film is a critical factor for optimizing particle removal performance.

3.4.2 Determination of Air Cleaning Factor and Negative Ion Concentration

The ACF is computed using the formula **[23, 24]**,

$$\mathrm{ACF} = \frac{\mathrm{CNatural\ (Pm, t)}}{\mathrm{CEAP\ (Pm, t)}} \ldots\ldots\ldots\ldots\ldots\ldots\ldots\ldots\ldots\ldots\ldots (4)$$

The ACF which quantifies the effectiveness of particle removal through ion emission, was calculated for EAPs using SS and Cu films. **Fig. 9** shows Air cleaning factor verses time at various bath concentration for dhoop PM. It shows that the ACF is higher for Cu films compared to SS. As the Cu bath concentration increases from 0.025 M to 0.075 M, the ACF rises from 6.57 to 48.55, whereas it decreases to 9.03% at 0.100 M. The highest ACF is observed for the CC_3 based EAP, which is significantly greater than that of the SS EAP.

A key factor in assessing an air purifier's performance is the rate of ion generation. A negatively polarized ion generator was chosen due to its advantages. **Fig. 10** shows the negative ions concentration against time with various solvent concentration for dhoop PM. It was observed that the CC_3 thin film used as the discharging electrode in the EAP produces higher concentrations of air ions compared to SS or other electrodes. Furthermore, it shows that, unlike other types of EAPs, the CC_3 based EAP maintains a relatively consistent ion emission over time. The concentration of negative ions over time was measured for dhoop PM at different bath concentrations.

4. Conclusion

The effect of solution concentration on the physical, chemical, and air-purifying properties of Cu films was investigated. XRD analysis confirms that the Cu films possess a FCC crystal structure. SEM images reveal that the CC_3 film, prepared at a 0.075 M bath concentration, exhibits a nodular morphology with small pores, formed due to the irregular orientation and aggregation of the nodules. The nodules on the CC_3 film have sizes ranging from 48 to 67 nm. This type of surface

increases the overall surface area and promotes enhanced ion emission through its pores, thereby improving the air purifying performance of the film. AFM analysis shows that as the bath concentration increases from 0.025 M to 0.075 M, the mean particle size of the Cu films increases from 86.52 to 224.55 nm, and the RMS surface roughness increases from 23.44 to 76.19 nm. However, at a 0.100 M solution concentration, both the RMS roughness and mean particle size decrease to 45 nm and 168.5 nm, respectively. The CC_3 thin film, synthesized at a solution concentration of 0.075 M and with a thickness of 721 nm, achieves the highest particle removal efficiency (PRE) of 88.78% and an ACF of approximately 54.12 after 405 sec of EAP operation for dhoop. These values are significantly higher than those for the SS discharging plate. All types of EAPs emit a small amount of ozone (O_3), but the concentration is well below the harmful human exposure limits, making the system safe to use while benefiting from its air purification capabilities. Additionally, it is demonstrated that in a closed and unventilated room, the CC_3 based EAP reduces PM_{10} and $PM_{2.5}$ concentrations from hazardous to acceptable levels within 45 and 90 sec, respectively. The CC_3 film generates the highest number of negative air ions compared to SS and other Cu films produced at varying bath concentrations. The physical and chemical properties of the Cu film show that as the bath concentration increases, the surface morphology, crystal structure, and surface roughness improve, creating a larger and more dynamic surface area for ion emission. Consequently, the enhanced physical chemical characteristics of the CC_3 EAP lead to a higher surface area for ionic discharge, which boosts the particle removal rate, ion production rate, air purification factor, and PM disintegration rate for dhoop PM. These improvements contribute to a healthier indoor environment.

Conflict of interest statement

The authors declare that they have no known competing financial interests or personal relationships that could have appeared to influence the work reported in this paper.

Data availability statement

Data will be made available on reasonable request.

Credit authorship contribution statement

R. S. Sidharaddi: Conceptualization, Data curation, Investigation, Methodology, Validation, Writing - original draft; **A. A. Mane:** Conceptualization, Review & editing; **P. S. Maldar:** Conceptualization, Review & editing; **S. P. Desai:** Conceptualization, Review & editing; **M. H. Nadaf:** Conceptualization, Review & editing; **A. B. Farakte:** Conceptualization, Review & editing; **A. S. Selmokar:** Conceptualization, Review & editing; **S. A. Nikam:** Conceptualization, Review & editing; **V. S. Sawant:** Conceptualization, Supervision, Review & editing.

Acknowledgment

The authors would like to acknowledge the SAIF and PIFC, Department of Physics, Shivaji University, Kolhapur, and YCIS, Satara, for providing research facilities and material characterization support.

Funding Declaration

This research received no specific grant from any funding agency in the public, private, or not-for-profit sectors.

References

[1] A. Goel, R. Wathore, T. Chakraborty, M. Agrawal, Characteristics of exposure to particles due to incense burning inside temples in Kanpur, India, Aerosol Air Qual. Res. 17 (2017) 608-615

[2] A. J. Petkus, D. Younan, K. Widaman , M. Gatz , J. E. Manson , X. Wang , M. Serre , W. Vizuete, H. Chui, M. A. Espeland, S. Resnick, J. C. Chena, Exposure to fine particulate matter and temporal dynamics of episodic memory and depressive symptoms in older women, Environ. Int.l 135 (2020) 105196

[3] J. H. Sung, Y. Lee, B. Han, Y. J. Kim, H. J. Kim, Improvement of particle clean air delivery rate of an ion spray electrostatic air cleaner with zero-ozone based on diffusion charging, Build. Environ.186 (2020) 107335

[4] S. Shen, W. Zhu, Y. Peng, F. Hai, J. Feng, Y. Deng, Highly Conductive and Fatigue-Free Flexible Copper Film Electrode Fabricated by a Facile Dry Transfer Technique, Adv. Mater. Interfaces 5 (2018) 1701038

[5] S. Cheng, J. Ye, Y. Zhao, Z. Huang, Y. Wang, Study on organic coating to improve the adhesion properties of Cu/Sn-plated bead wire and rubber, Int. J. Adhes. Adhes. 134 (2024) 103778

[6] W. Zhou, X. Ding, W. Li, L. Zhao, Y. Lu, M. Zhao, F. Ma, Z. Wen, H. Zhang, J. Feng, Copper deposition on MgO surfaces: Synergistic effect of multivalent Cu and oxygen vacancies efficiently activates H_2O_2 and enhances photo-Fenton efficiency, Colloids Surf. A: Physicochem. Eng. Aspects 731 (2026) 139074

[7] J. Bi, L. Yao, J. Ao, S. Gao, G. Sun, Q. He, Z. Zhou, Y. Sun, Y. Zhang, Pulse electro-deposition of copper on molybdenum for Cu(In, Ga)Se_2 and $Cu_2ZnSnSe_4$ solar cell applications, J. Power Sources 326 (2016) 211-219

[8] X. Wang, S. Wei, L. Xu, J. Li, X. Li, K. Shan, Preparation of w–cu nano-composite powders with high copper content using a chemical co-deposition technique, Adv. Powder Technol. 29 (6) (2018) 1323-1330

[9] N. Prudhomme, V. Constantoudis, A. E. Turgambaeva, V. V. Krisyuk, D. Samelor, F. Senocq, C. Vahlas, Chemical vapor deposition of Cu films from copper(I) cyclopentadienyl triethylphophine: Precursor characteristics and interplay between growth parameters and films morphology, Thin Solid Films 701 (2020) 137967

[10] Q. Wang, R. Yuan, M. Yang, W. Gao, S. Jiao, D. Tian, H. Jiao, H. Yu, D. Sun, Exploring coating electrodeposition protocols from a cross-electrolyte and cross-metal perspective, J. Mater. Sci. Technol., 226 (2025) 122-134
[11] M. S. Tovar-Oliva, I. Tudela, Electrodeposition of nano- and micro-materials: Advancements in electrocatalysts for electrochemical applications, Results Eng. 24 (2024) 103285
[12] E. Rudnik, Electrochemical and Electroless Deposition of High-Entropy Alloy Thin Films: A Review of Plating Conditions, Properties, and Applications, Appl. Sci. 15 (2025) 8009
[13] F. Yang, Q. Liu, G. Li, X. Zhang, S. B. Rozali, N. N. N. Ghazali, M. F. M. Sabri, H. Zhao, Effect of additives and optimized Cyclic voltammetry parameters on the morphology of electrodeposited Tellurium thin film, J. Electroanal. Chem., 925 (2022) 116872
[14] R. Hessam, P. Najafisayar, The effects of applied current density, bath concentration and temperature on the morphology, crystal structure and photoelectrochemical properties of electrodeposited hematite films, International Journal of Hydrogen Energy 44 (41) (2019) 22851-22862
[15] J. A. M. Oliveira, A. F. de Almeida, A. R. N. Campos, S. Prasad, J. J. N. Alves, R. A. C. de Santana, Effect of current density, temperature and bath pH on properties of Ni–W–Co alloys obtained by electrodeposition, J. Alloys Compd. 853 (2021) 157104
[16] X. Wu, X. Zhao, P. Lin, C. Tan, C. Wang, W. Chen, Effects of electrodeposition current density and additives on the microstructure and mechanical properties of copper films, J. Mater. Res. Technol. 36 (2025) 1789-1801
[17] S. J. Kim, J. Lee, Y. H. Choi, D. H. Yeon, Y. Byun, Effect of copper concentration in printable copper inks on film fabrication, Thin Solid Films 520 (2012) 2731-2734
[18] M. A. Yıldırım, The effect of copper concentration on structural, optical and dielectric properties of CuxZn1-xS thin films, Opt. Commun. 285 (2012) 1215-1220
[19] V. S. Sawant, Experimental studies on corona discharge ionization, IOSR Journal of Applied Physics 3 (2) (2013) 11-15
[20] Y. W. Hung, D. P. Tran, C. Chen, Effect of Cu ion concentration on microstructures and mechanical properties of nanotwinned Cu foils fabricated by rotary electroplating, Nanomaterials 11 (2021) 2135

[21] Y. Liao, H. Bai, F. Shi, J. Li, X. Liu, Influence of Film Thickness on the Structure and Properties of Copper Thin Films Deposited on BaTiO3 Ceramics by DCMS and HiPIMS, Materials 18 (2025) 5333
[22] H. Zhou, J. Wang, Z. Zhang, C. Q. Lan, High cell density culture of microalgae in horizontal thin-layer algal reactor: Modeling of light attenuation and cell growth kinetics, Chemical Engineering Journal 496 (2024) 154175
[23] V. S. Sawant, Experimental studies on corona discharge ionization, IOSR Journal of Applied Physics 3 (2) (2013) 11-15
[24] S. A. Grinshpun, G. Mainelis, M. Trunov, A. Adhikari, T. Reponen, K. Willeke, Evaluation of ionic air purifiers for reducing aerosol exposure in confined indoor spaces, Indoor Air, 15 (2005) 235-245
[25] B. Pushpawela, R. Jayaratne, A. Nguy, L. Morawska, Efficiency of ionizers in removing airborne particles in indoor environments, J. Electrost. 90 (2017) 79-84

Figure captions:

Fig. 1 Schematic of electrodeposition method

Fig. 2 Experimental setup of dhoop smoke with EAC

Fig. 3 XRD patterns of copper films deposited at different bath concentrations a) CC1 b) CC2 c) CC3 and d) CC4

Fig. 4 SEM images of Cu films deposited at different solution concentrations: a) CC1, b) CC2, c) CC3, and d) CC4

Fig. 5 SEM images of CC3 Cu thin film at different magnifications: i) x 2000, (ii) x 5000, (iii) x 10000, and (iv) x 20000

Fig. 6 The AFM micrographs of Cu films deposited at different bath concentrations a) CC1, b) CC2, c) CC3, and d) CC4

Fig. 7 Concentration of particles versus time for dhoop particulate matter using EAP

Fig. 8 Efficiency for removing particles verses time of dhoop PM for various concentrations of solvents

Fig. 9 Air-cleaning factor verses time at various bath concentration for dhoop PM

Fig. 10 The negative ions concentration against time with various solvent concentration for dhoop PM

Table captions:

Table 1 The crystallite size, thickness of film, mean particle size and RMS roughness for electrodeposited Cu films prepared at various bath concentration

Table 2 Reaction time for 80 % declining smoke PM, duration for 50% visibility, PRE after 120 s working of EAP and ACF

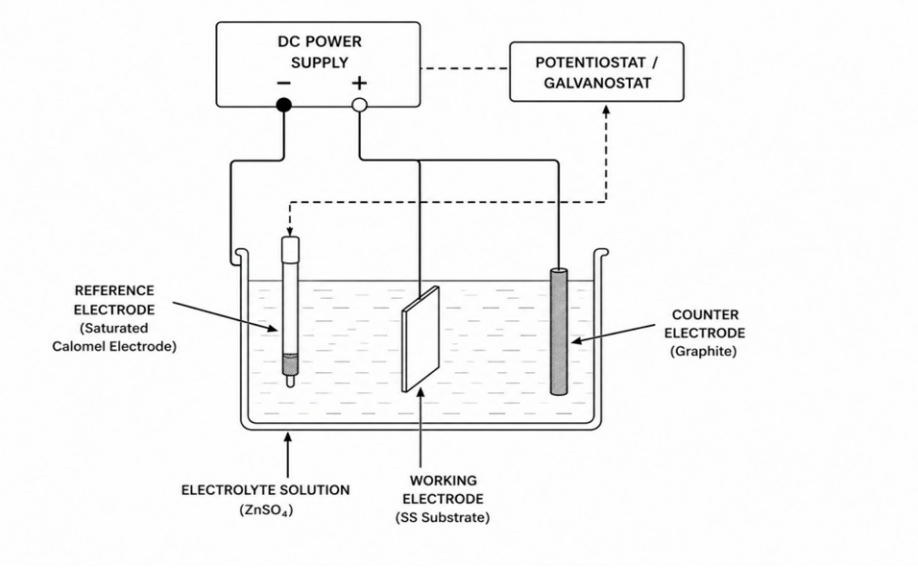

DC POWER SUPPLY
−
+
POTENTIOSTAT / GALVANOSTAT
REFERENCE ELECTRODE (Saturated Calomel Electrode)
COUNTER ELECTRODE (Graphite)
ELECTROLYTE SOLUTION ($ZnSO_4$)
WORKING ELECTRODE (SS Substrate)

Fig. 1

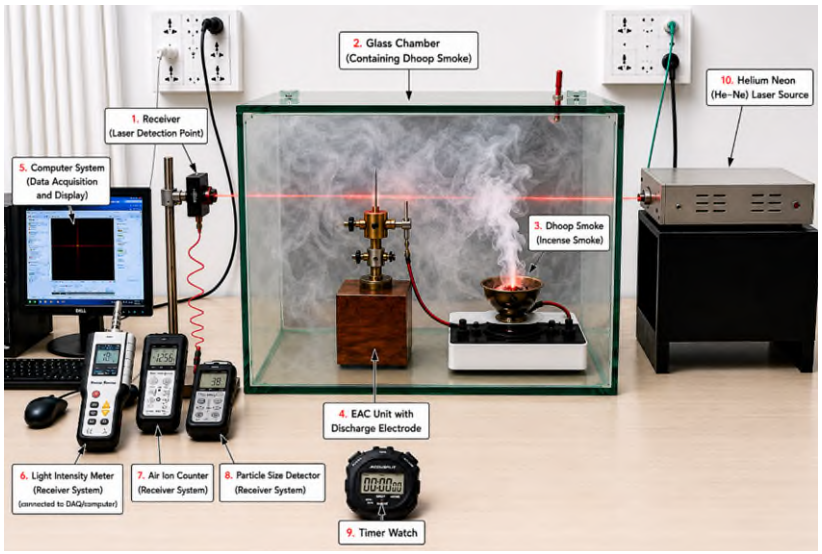

2. Glass Chamber (Containing Dhoop Smoke)
10. Helium Neon (He-Ne) Laser Source
1. Receiver (Laser Detection Point)
5. Computer System (Data Acquisition and Display)
3. Dhoop Smoke (Incense Smoke)
4. EAC Unit with Discharge Electrode
6. Light Intensity Meter (Receiver System) (connected to DAQ/computer)
7. Air Ion Counter (Receiver System)
8. Particle Size Detector (Receiver System)
9. Timer Watch

Fig. 2

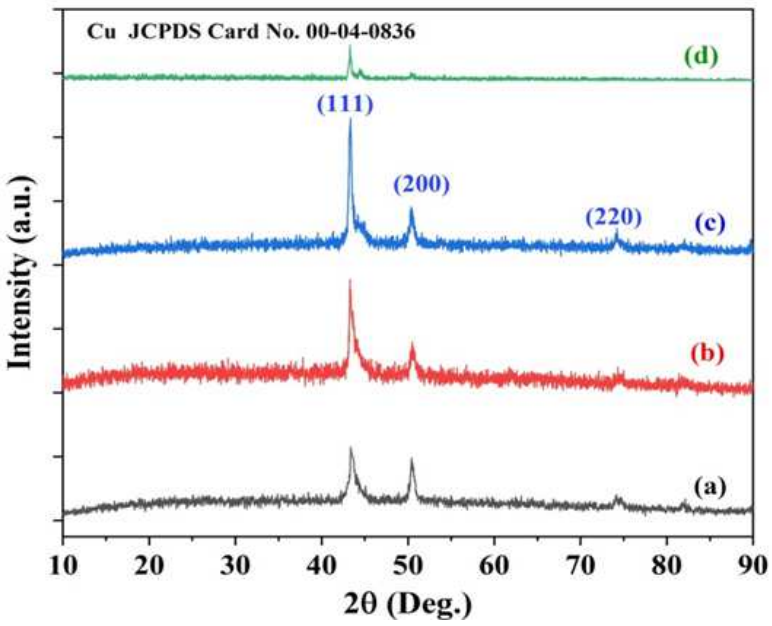

Cu JCPDS Card No. 00-04-0836
(d)
(111)
(200)
(220)
(c)
(b)
(a)
Intensity (a.u.)
10
20
30
40
50
60
70
80
90
2θ (Deg.)

Fig. 3

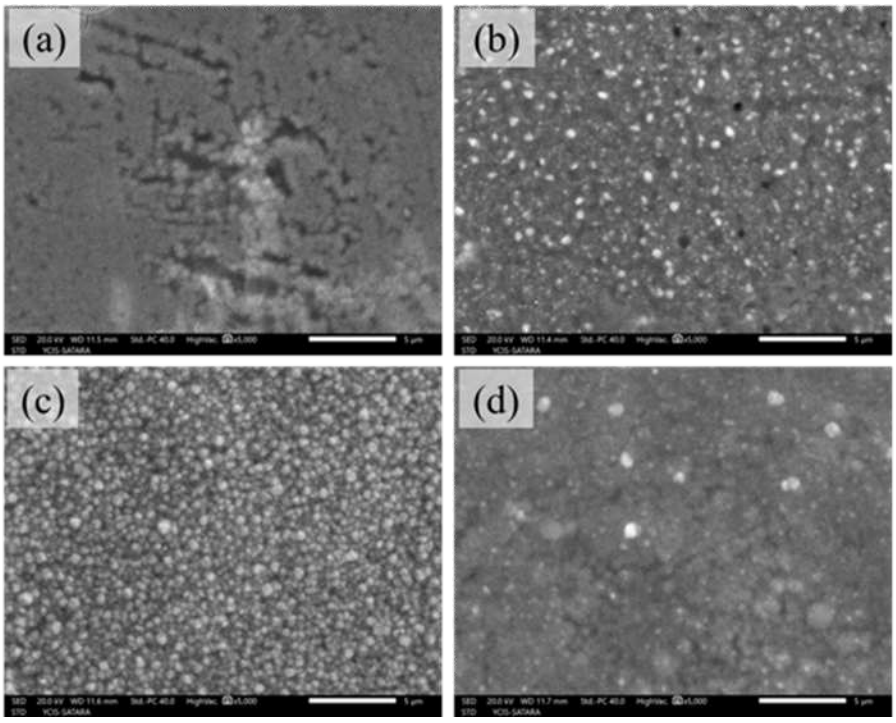

(a)
(b)
(c)
(d)

Fig. 4

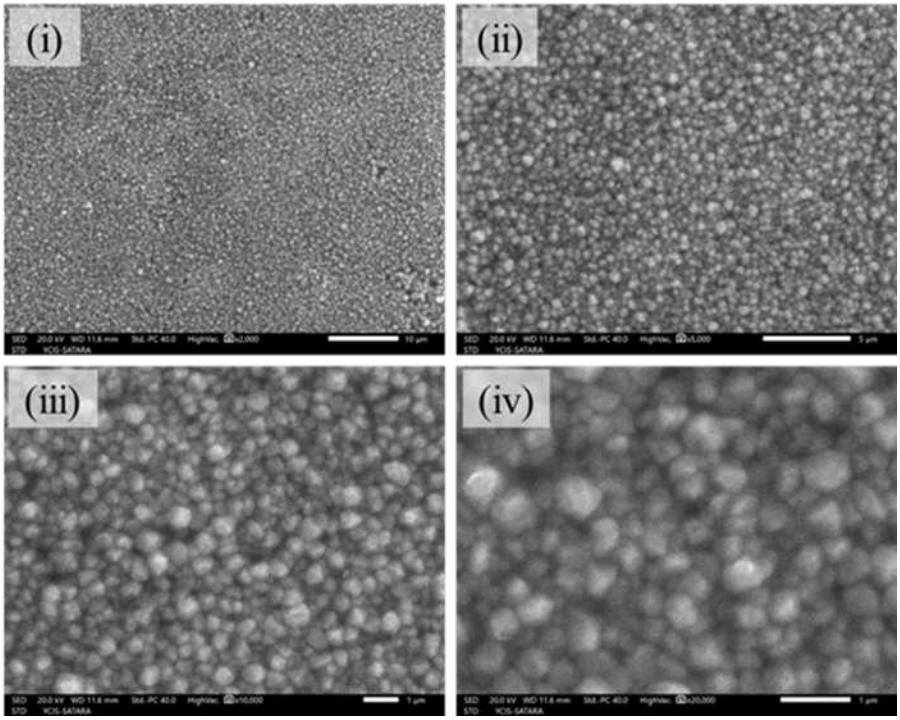


Fig. 5

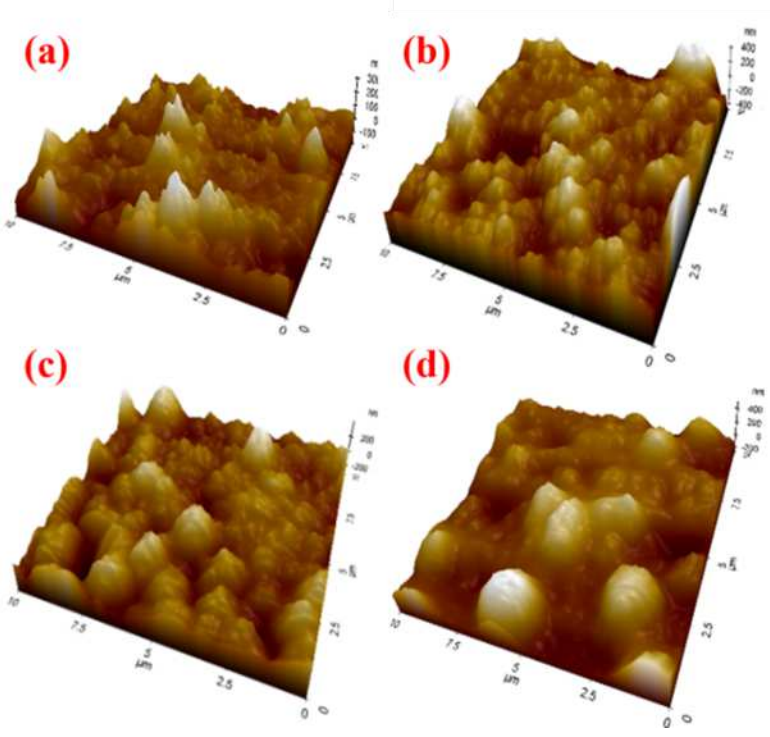


Fig. 6

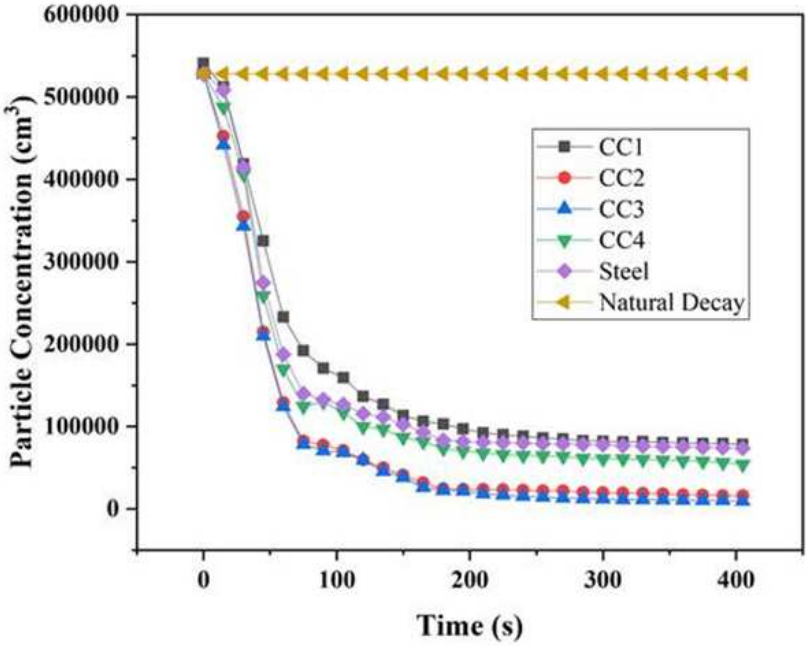

Particle Concentration (cm^3)
600000
500000
400000
300000
200000
100000
0
0
100
200
300
400
Time (s)
CC1
CC2
CC3
CC4
Steel
Natural Decay

Fig. 7

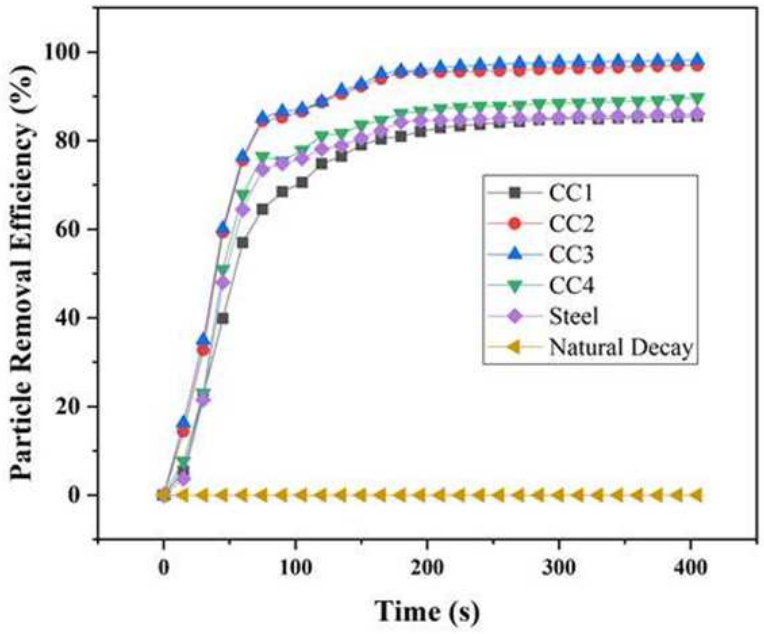

Particle Removal Efficiency (%)
100
80
60
40
20
0
0
100
200
300
400
Time (s)
CC1
CC2
CC3
CC4
Steel
Natural Decay

Fig. 8

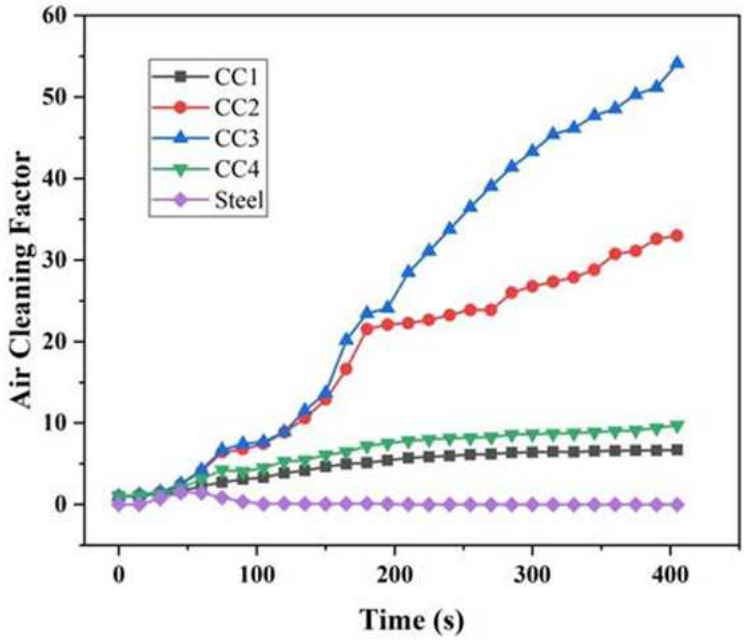

Air Cleaning Factor
Time (s)
CC1
CC2
CC3
CC4
Steel
0
10
20
30
40
50
60
0
100
200
300
400

Fig. 9

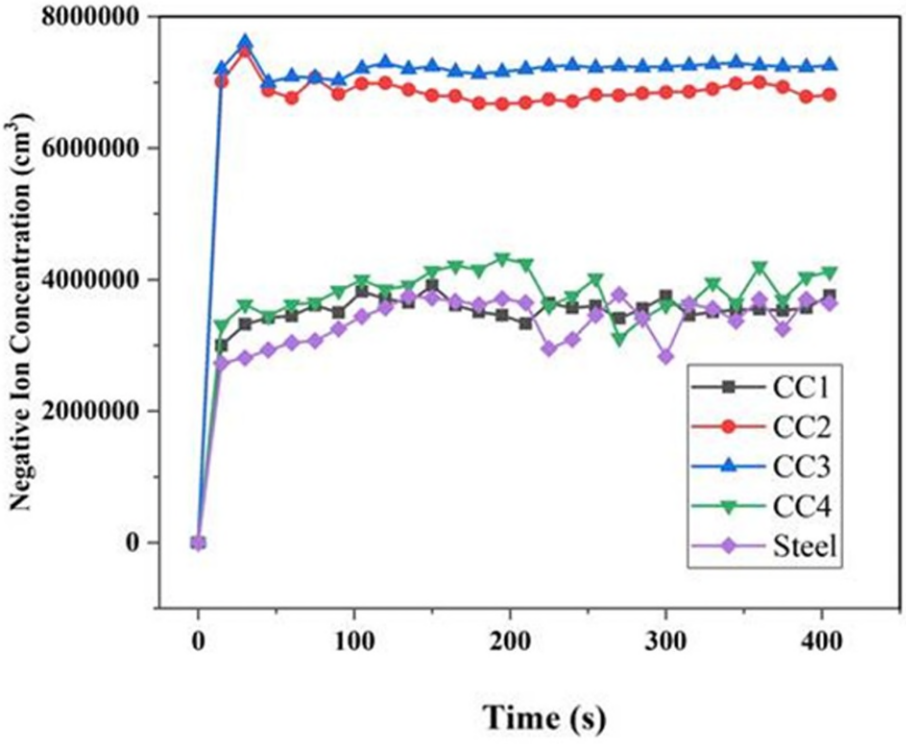

Negative Ion Concentration (cm^3)
Time (s)
CC1
CC2
CC3
CC4
Steel
0
2000000
4000000
6000000
8000000
0
100
200
300
400

Fig. 10

Table 1

Sample-codes	XRD results	Thickness of film (nm)	AFM results	
	Crystallite size of (111) plane (nm)		Mean particle size (nm)	RMS surface roughness (nm)
CC_1	52.3	562	86.52	23.44
CC_2	61.1	633	209.58	64
CC_3	62.7	721	224.55	76.19
CC_4	34.6	756	168.5	45

Table 2

Type of EAP	Reaction time for declining 80 % smoke PM (s)	Duration for 50 % visibility (s)	ERP after 120 s EAP working (%)	ACF at different time (s)		
				120	240	360
CC1	180	150	74.77	3.86	5.97	6.57
CC2	75	80	88.69	8.84	23.20	30.74
CC3	75	75	88.78	8.91	33.79	48.55
CC4	120	120	81.09	5.28	8.14	9.03
CC5	150	120	78.11	4.56	6.6	6.99